The critical current density of grain-boundary channels in polycrystalline HTS and LTS superconductors in magnetic fields

P Sunwong, J S Higgins, Y Tsui, M J Raine and D P Hampshire

Department of Physics, Superconductivity Group, Centre for Materials Physics, University of Durham, South Road, Durham DH1 3LE, United Kingdom

PACS codes: 74.20.De Phenomenological theories (two-fluid, Ginzburg-Landau, etc.); 74.25.Sv Critical currents; 74.45.+c Proximity effects, Andreev effect, SN and SNS junctions;

Date submitted: 20th June 2013

Published version:
P. Sunwong, J. S. Higgins, Y. Tsui, M. J. Raine and D. P. Hampshire - The critical current density of grain boundary channels in polycrystalline HTS and LTS superconductors in magnetic fields - SUST 26 095006 (2013)

Correspondence e-mail: d.p.hampshire@durham.ac.uk

Abstract

We provide evidence that a single mechanism - flux flow along channels – can explain the functional form of the critical current density (J_c) in the low temperature superconductor Nb_3Sn and in the high temperature superconductors (HTS) $YBa_2Cu_3O_{7-\delta}$ (YBCO) and $(Bi,Pb)_2Sr_2Ca_{n-1}Cu_nO_x$ (BiSCCO) in low and high magnetic fields. In this paper, we show that standard flux pinning theories, used for the last four decades to describe J_c in low temperature superconductors (LTS), cannot explain the strain dependence of J_c in YBCO because J_c is a function of strain but the average superconducting properties are not. We conclude that in the polycrystalline samples presented here, the channels are grain boundaries that are narrow and metallic in Nb_3Sn and YBCO but wide and semiconducting in BiSCCO. Strain alters J_c by changing the superconducting properties of the grains in Nb_3Sn but by changing the grain boundaries in YBCO.

1. INTRODUCTION

A description of the long-standing approach used to increase the critical current density (J_c) of polycrystalline low temperature superconductors (LTS) such as Nb_3Sn[1] in high magnetic fields, is probably best encapsulated by the flux pinning scaling laws used to parameterise the volume pinning force F_p and J_c given by [1, 2]

$$F_p = J_c \times B = \frac{\alpha}{D} B_{c2}^n \left(\frac{B}{B_{c2}}\right)^p \left(1 - \frac{B}{B_{c2}}\right)^q, \quad (1)$$

where α, n, p and q are constants, D is the grain size, B the applied field and B_{c2} is the upper critical field. For Nb_3Sn, this functional form best fits the data in fields above 1 or 2 T. The intrinsic properties of materials have been improved by doping to increase B_{c2} [3]. The extrinsic properties have been improved by reducing the grain size to increase the density of grain boundaries or adding precipitates, which increases the pinning and hence J_c, and by changing the pinning mechanism operating to optimise p and q [4]. These approaches have successfully provided materials that enable applications from body scanners to the Large Hadron Collider[5]. However, the discovery of the weak-link problem in high temperature superconductors (HTS)[6] including the exponential decay of J_c in high fields, suggested that transmission of supercurrent through the grain boundaries limits J_c in HTS such as $YBa_2Cu_3O_{7-\delta}$ (YBCO)[7, 8]. This has meant that scientists developing HTS have adopted a different strategy to that used for LTS and focussed on the formidable challenge of producing km-long quasi-single crystalline materials with only (and as few as possible) low-angle grain boundaries[9]. In this paper we show that in the polycrystalline materials presented here, flux flow along grain boundaries can explain the functional form of J_c in both high and low fields in both LTS and HTS. Although it has long been known that flux-flow along grain boundaries is a possible description of dissipation in polycrystalline superconductors, the many forces on the fluxons that operate in these materials and complex disorder in the flux-line-lattice have meant that until computational visualisation of flux flow was obtained[10] (using Time Dependent Ginzburg Landau (TDGL) theory), there was no strong evidence that this is the dissipative state. Furthermore, there has been no mathematical framework to describe such dissipation. Recently in our group, we have found analytic solutions that describe J_c for superconducting-normal-superconducting (SNS) junctions in high fields[11]. They are used here to model polycrystalline superconductors as a collection of such junctions. We present J_c measurements obtained as a function of field, temperature, angle of field and strain for (polycrystalline) Nb_3Sn wire, YBCO tape and BiSCCO tape and show that a single mathematical framework describes the data.

2. FLUX FLOW ALONG GRAIN BOUNDARIES

In low magnetic fields, J_c through a narrow SNS junction, is given by the familiar sinc function[12, 13]

$$J_c = \frac{\hbar J^*(0)}{2ew\ \ d+\lambda_{(S)}\ \ B}\left|\sin\frac{2ew\ \ d+\lambda_{(S)}\ \ B}{\hbar}\right|, \tag{2}$$

where w is the width of the junction, $d+\lambda_{(S)}$ is known as the effective half-thickness of the junction and the penetration depth is $\lambda_{(S)}$. Since we consider anisotropic materials here, we distinguish parameters that are determined by the direction of current flow by an uppercase star (associated with the effective mass of the carriers) from those determined by the angle of the applied field with respect to the crystallographic axes (eg B^*_{c2} and B_{c2}). Equation (2) does not consider the complex spatial variation of the order parameter in the mixed state where fluxon formation occurs in the junction and in the superconductor. TDGL computation in our group (on isotropic superconductors) has confirmed that for wide junctions or in high magnetic fields where many fluxons are in the junction, the sine term, which is associated with the phase of the superelectrons, is averaged out to $1/\sqrt{2}$ [11] (and we assume this averaged value remains correct for the highly textured HTS materials considered in this work). When the superconductor is in the mixed state and the magnetic field produces many fluxons in the junction, the factor $d+\lambda_{(S)}$ is replaced by $d+\xi_{(S)}$. Complimentary analytic work has led to a general solution for the depairing current J_{D-J} through one-dimensional SNS junctions[11] that accounts for the depression of the order parameter by magnetic field and is given by

$$J_{D-J} = \frac{\rho_S}{\rho_N}\frac{B^*_{c2}}{\mu_0\lambda^*_S\kappa^*}\hat{\psi}^2_\infty\left(\frac{B}{B_{c2}}\right)^{\frac{1}{2}}\left(\frac{2B}{B_{c2}}\frac{d^2}{\xi^2_{(S)}}+\frac{1}{\gamma}\right)^{\frac{1}{2}}F^2\exp\left(-\frac{B\gamma}{B_{c2}}\frac{d^2}{\xi^2_{(S)}}\right) \tag{3}$$

where

$$F = \left[\sqrt{\left(\frac{\rho_S}{\sqrt{2}\rho_N}\frac{B\gamma}{B_{c2}}\frac{d}{\xi_{(S)}}\left(1-\frac{1}{\frac{2B\gamma}{B_{c2}}\frac{d^2}{\xi^2_{(S)}}+1}\right)\right)^2}+1-\frac{\rho_S}{\sqrt{2}\rho_N}\frac{B\gamma}{B_{c2}}\frac{d}{\xi_{(S)}}\left(1-\frac{1}{\frac{2B\gamma}{B_{c2}}\frac{d^2}{\xi^2_{(S)}}+1}\right)\right], \tag{4}$$

$\hat{\psi}^2_\infty = (1-b)$, $\gamma^2 = (1+eBd^2/\hbar)/(6+eBd^2/\hbar)$, $\kappa = \lambda_{(S)}/\xi_{(S)}$ is the Ginzburg-Landau parameter and $\rho_{(S)}$ and $\rho_{(N)}$ are normal state resistivities of the superconducting grains and the normal grain boundaries respectively[14]. Note the form of $\frac{B\gamma}{B_{c2}}\frac{d^2}{\xi^2_{(S)}}$ is used for convenience and does not strongly depend on the superconducting properties since it is equal to $\frac{2eB\gamma d^2}{\hbar}$. $J^*(0)$ in (2) can then be equated to J_{D-J} of the junction which gives:

$$J_c\ \ B\ \approx \frac{1}{\sqrt{2}}\frac{B^*_{c2}}{\mu_0\xi^*_S(\kappa^*)^2}\frac{r\xi^2_S}{w\ \ d+\xi_S}\left(\frac{1}{b}\right)^{\frac{1}{2}}\left(\frac{2bd^2}{\xi^2_{(S)}}+\frac{1}{\gamma}\right)^{\frac{1}{2}}.F^2.\ 1-b\ \exp\left(-\frac{b\gamma d^2}{\xi^2_{(S)}}\right) \tag{5}$$

where we have used dimensionless units $r = \frac{\rho_S}{\rho_N}$ and $b = \frac{B}{B_{c2}}$. In high fields, we find experimentally (below) that d is equal to a few coherence lengths[15, 16] where

$$d = s[\xi_{(S)}(T) - d_0] \tag{6}$$

and s and d_0 are constants. Our approach is phenomenological so the details of microscopic processes are neglected[17] and the parameters derived are assumed to be characteristic averages of the distributions of materials properties that inevitably occur in inhomogeneous high J_c materials. We have not included the De Gennes[18] exponential term that characterises the decay of the order parameter in zero-field across a thick junction[11] because it is not required to fit the J_c data presented in this paper. The central proposition of this paper is that we can consider LTS and HTS polycrystalline superconductors as a collection of SNS junctions where equations (5) and (6) describe J_c in high and low magnetic fields and above criticality, flux flows along grain-boundary channels.

3. SAMPLES AND EXPERIMENTAL TECHNIQUES

Three different types of samples were measured: Multifilamentary DI-BiSCCO type HT tapes supplied by Sumitomo Electric Industries. The average width and thickness of the tapes were 4.5 mm and 0.36 mm, respectively; YBCO tapes from SuperPower (SCS4050). The superconducting layer was deposited onto a Hastelloy substrate with buffer layers, using a metal organic chemical vapour deposition technique, and stabilised by a copper layer. The superconducting YBCO layer was approximately 4 mm wide and 1 μm thick; Nb_3Sn wires manufactured by Bruker EAS using the multifilamentary bronze-route process. The average diameter of the wires was 0.81 mm.

The magnetisation J_c measurements and ac magnetic susceptibility measurements of YBCO, BiSCCO and Nb_3Sn were completed in a Quantum Design Physical Properties Measurement System© in magnetic fields up to 8.5 T at different temperatures. In the magnetisation measurements, hysteresis loops were obtained and the magnetisation J_c was calculated using Bean's critical state model[19]. Ac magnetic susceptibility measurements were also used to find $B_{c2}(T)$.

The transport J_c measurements of Nb_3Sn were made using a standard four-terminal technique and the critical currents were determined using a 10 μVm^{-1} electric field criterion. J_c for YBCO and BiSCCO was determined at 100 μVm^{-1}. The critical current densities were calculated using the critical current divided by the unstrained cross-sectional area of the superconducting components. Transport J_c measurements on Nb_3Sn wires were performed at 4.2 K in magnetic fields up to 14.5 T in a vertical superconducting magnet using our purpose-built strain probe which includes a copper beryllium spring sample holder[20, 21]. The measurements of YBCO and

BiSCCO tapes were performed at 77 K in magnetic fields up to 0.7 T in a conventional iron-cored electromagnet and at 4.2 K in magnetic fields up to 14 T in a 40-mm-bore horizontal split-pair superconducting magnet at different angles between the field and the tape surface. The strain measurements were carried out by using a springboard-shaped copper beryllium sample holder for applying strains up to 0.3 % in tension and -1.3 % in compression [22, 23].

4. EXPERIMENTAL FUNCTIONAL FORM OF J_c

Figure 1 shows magnetisation J_c as a function of applied magnetic field and identifies what we call in this work the self-field regime, the power-law regime and the exponential regime. The solid lines are fits to the data using equations (5) and (6) where we have assumed that the Ginzburg Landau constants are 33, 94 and 139 for Nb_3Sn, YBCO and BiSCCO respectively[24]. At the very lowest fields, the (log-log) insets of figure 1 show that J_c is field-independent and the range over which J_c is field-independent decreases as temperature increases. This is consistent with the self-field produced by the flowing current being much higher than the external magnetic field. At low fields, $J_c(B)$ shows power-law behaviour with an exponent of -0.5, consistent with equation (5). The power-law behaviour occurs over a wider range of fields and temperatures for YBCO than Nb_3Sn and BiSCCO and is attributed (below) to thinner grain boundaries. At sufficiently high fields, there is a cross-over from the power-law to the exponential regime which has been observed experimentally by other authors[25-28]. We note that in other (lower J_c) YBCO samples, $J_c(B)$ is exponential over several orders of magnitude and a much larger range of field and temperature phase space[29] than shown here, which is consistent with attributing the field dependence to the nature of the grain boundaries and not the intrinsic properties of any specific superconducting material.

The functional form of $B_{c2}(T)$ has been derived for each of the three materials studied here from fitting the J_c data to equations (5) and (6). In figure 2, we have compared these functional forms with B_{c2} values from the literature, as well as with those obtained from in-house ac magnetic susceptibility measurements. B_{c2} has been characterised at 1%, 5% and 50% of full screening M'_{fs} in order to quantify how sensitive the values are to the criterion used. For Nb_3Sn (one of the important superconducting materials used in the ITER tokamak[30]), there is an enormous amount of data in the literature on samples fabricated by different routes and with different microstructure. $B_{c2}(T)$ obeys the WHH equation and can be characterised by $B_{c2}(T) = B_{c2}(0)(1-t^{1.5})$, where $t = T/T_c$ is the reduced temperature[31-33]. The data at 1% of screening give values of $B_{c2}(0)$ and T_c of 26.3 T and 16.7 K which are similar to those derived from the J_c data ($B_{c2}(0)$ and T_c are 26.3 T and 16.2 K), and the literature data. For HTS, the fundamental properties and their variation with sample preparation and microstructure are far less well known, particularly at low temperatures where $B_{c2}(T)$ values are high. Nevertheless for YBCO, pulsed field $B_{c2}(T)$ data available up to 400 T [34] are shown in figure 2(d). We have used $B_{c2}(T) = B_{c2}(0)(1-t^{0.61})$ to fit the J_c data with values of $B_{c2}(0)$ and T_c of 68.5 T and 87.6

K, which only differs significantly from the pulsed field temperature dependence at 25 K and below where we find an upward curvature in B_{c2}. This curvature may arise from the difference in magnitude of $B_{c2}(0)$ between the single crystal sample used for pulsed field measurements and our tape, optimised for high J_c, or our assumption that κ is independent of temperature. A concave curvature of $B_{c2}(T)$ has been observed in several BiSCCO systems[35-37] which can be characterised using a scaling function $B_{c2}(T) = B_{c2}(0)(1-t^{0.5})^{2.1}$, where fitting parameters from the J_c data for our BiSCCO sample are $B_{c2}(0)$= 84.5 T and T_C = 110.8 K. The data in figure 2 show that there is reasonably good agreement between the reduced temperature dependence and the free parameters obtained from different measurements on different samples. For BiSCCO, the current densities are a significantly smaller fraction of the depairing current density than in say YBCO. When fitting the BiSCCO data at low fields, we find that unlike Nb_3Sn or YBCO, the temperature dependence for J_c cannot be explained by the temperature dependence of B_{c2} alone. We attribute the different behaviour of BiSCCO to the temperature dependence of r and describe it empirically by $r(T) = r_0 \exp(T/T_0)$ where $r_0 = 3.6 \times 10^{-2}$ and T_0 = 36 K in the fits to the data. The temperature dependence of r is consistent with ρ_N (associated with the grain boundary) increasing with decreasing temperature. Also shown in figure 2 are values of $\beta(T)$. We found $\beta(T)$ for all three materials by assuming that in the high field regime, in fields not too close to $B_{c2}(T)$, we can simply consider J_c to be proportional to $\exp -B/\beta(T)$. For YBCO, we did not make measurements in sufficiently high magnetic fields to reach the high-field exponential regime at low temperatures. Nevertheless the data in figure 2 show the temperature dependence of $\beta(T)$ is similar to $B_{c2}(T)$ for all three materials (where comparison is available) and has led to the empirical equation (6).

The anisotropy of YBCO and BiSCCO can be described using anisotropic Ginzburg-Landau theory which relates the angle θ between the magnetic field and the a-b plane of the crystal structure using $B_{c2}(\theta) = B_{c2}(\pi/2).(\sin^2\theta + \Gamma^{-2}\cos^2\theta)^{-\frac{1}{2}}$ [38], where Γ characterises the degree of anisotropy. Here we treat YBCO and BiSCCO as anisotropic layered superconductors with three-dimensional behaviour. Although weak Josephson coupling between superconducting layers in BiSCCO leads to two-dimensional behaviour at low temperature and is described most accurately using Lawrence-Doniach theory[39], the B_{c2} values calculated from these two theories are only significantly different at very low θ and are almost indistinguishable for very highly anisotropic materials and the data considered here.

We have measured J_c as a function of field, strain and angle at 77 K and 4.2 K in a standard vertical magnet (Nb_3Sn) and a horizontal split-pair magnet (YBCO and BiSCCO) using dedicated probes designed in-house for transport measurements. Current flow is orthogonal to the field at all angles. These transport experiments are particularly demanding in the split-pair magnet at 4.2 K because of the large forces on the samples. However, the angular measurements have the advantage that unlike angular magnetic measurements, the interpretation of the data is more straightforward because the path of the macroscopic current flow is unambiguous. In figure 3, the angular dependence of J_c is shown. Equation (5) implies

that universal scaling behaviour should be observed for the angular dependence of J_c as a function of $B.(\sin^2\theta+\Gamma^{-2}\cos^2\theta)^{\frac{1}{2}}$. This universality is confirmed as a function of angle at several magnetic fields for YBCO at 4.2 K and at three different strains as a function of field and angle for BiSCCO. We attribute the relatively small asymmetry about 0 degrees at 4.2 K (Fig. 3b) and at 77K (not shown) for YBCO predominantly to angular hysteresis[40] and pinning (cf section 5). The anisotropy constant Γ obtained for YBCO and BiSCCO is 7.0 and 7.8 respectively, which are both within the range of values quoted in the literature. The YBCO sample used in this work was fabricated by deposition of YBCO film onto substrates with relatively good crystallographic alignment (misalignment less than 10° FWHM)[41] consistent with literature values for the anisotropy constant of 3 – 8 [12, 42, 43]. For BiSCCO, the anisotropy is at the low end of the range reported in the literature (Γ = 3 – 150 [44-47]). We attribute the value of Γ predominantly to anisotropy, but it is also affected by grain misalignment, which is important in BiSCCO since the tape was produced by the powder-in-tube (PIT) method. In both tapes the c-axis is preferentially orthogonal to the surface of the tape.

Figure 4 shows the normalised critical current density J_n (where $J_n = J_c(\varepsilon_a)/J_c(\varepsilon_p)$) versus strain. Relative strain (ε_r) is defined by: $\varepsilon_r = \varepsilon_a - \varepsilon_p$, where ε_a is the applied strain, and ε_p is the value of strain at which J_c reaches its peak value. For Nb_3Sn, there is the very strong field dependence expected for the strain dependence of J_n over the reduced field B/B_{c2} range 0.3 to 0.5. The strong effect of strain on the critical current density in LTS is attributed to the strong strain dependence of the superconducting properties B_{c2} and T_c and has been established for many Nb_3Sn samples in the literature[48].

For YBCO, J_c is shown for both B parallel and orthogonal to the c-axis of the samples at 77 K as a function of strain. At 4.2 K, measurements as a function of strain were only made with B oriented parallel to the c-axis to keep currents below 500 A. The strain at which the maximum value of $J_c(\varepsilon_p)$ occurred, changed from -0.3 % at 2 T to -0.1 % at 14 T as has been reported before[49] (although we saw no such change at 77K, nor did we see the double-peak in J_c versus strain observed elsewhere[49, 50]). We attribute these changes to the field and strain dependence of the grain boundaries' normal state properties. Unlike Nb_3Sn, the normalised J_c for YBCO is an almost universal function of relative strain, independent of magnetic field over a large range of B/B_{c2} from ~0.06 to 0.4 at 4.2 K, and both field and angle at 77 K. These results mean that B_{c2} and s are unaffected by strain (and from WHH theory[31] $\rho_{(S)}$ also) at these temperatures. At 77 K, the anisotropy constant Γ (characterised over a range of 70°) is also confirmed to be independent of strain for YBCO (figure 4c) and BiSCCO (inset to figure 3c). We conclude that the strain dependence of J_c is due to the strain dependence of r and hence $\rho_{(N)}$. Measurements of $\rho_{(N)}$ are required to explain why the strain dependence of r is larger at 77 K than 4.2 K and may require inclusion of the role of grain boundary dislocations as a function of strain[51]. We note that since flux pinning theories do not include normal state properties, they cannot explain the variable-strain J_c data presented here in Figs 4b and 4c for

YBCO at all. Given the data show that B_{c2} is unaffected by strain, if one used a flux pinning description given by equation 1, a parameterisation of the variable-strain J_c data would require a change in the grain-size by a factor 5 at 77 K, which is clearly not physical. In figure 4(b), we show how the strain dependent r eventually causes the universal behaviour to break down (in the high-field exponential regime) and leads to a less strain-dependent normalised J_c on approaching B_{c2}. Since B_{c2} is independent of strain at both 4.2 K and 77 K, we can expect that T_c is also strain independent. Because J_c is a complex parameter, determined by a range of different local properties including anisotropy, grain orientation, local defect and compositional properties, and grain boundary structures, the fitting parameters derived here are sample averaged and one can expect percolative current flow in a twinned YBCO tape. Single-crystal data on YBCO show that T_c increases with pressure along the *b*-axis and decreases with pressure along the *a*-axis with an average that is close to strain independent[52]. Hence the single-crystal data on YBCO suggest that although the average superconducting properties are strain independent, the underlying width of the distribution of the properties may change.

For BiSCCO, we found that accurate measurements of the strain dependence of J_c are demanding because the changes in J_c over the range of strain where J_c is reversible are much smaller than found in YBCO or Nb_3Sn. In the inset to figure 4(d), we show the 'roof-top' behaviour for J_c versus strain which we have characterised in the reversible strain region using the change in the normalised J_c with strain (at zero applied strain) as a function of reduced field $B/B_{c2}(90°)$. For B//a-b at 77 K and B // c-axis at 4.2 K, data are only available over a limited range of reduced field, J_c is in the power-law regime and we find $\mathrm{d}J_n/\mathrm{d}\varepsilon_a$ is almost independent of magnetic field. As with the YBCO data, this suggests that at least in this orientation, B_{c2} and s are unaffected by strain. However for B//c at 77 K, J_c is in the exponential regime and $\mathrm{d}J_n/\mathrm{d}\varepsilon_a$ is increasingly strain sensitive as the applied field increases. This increase cannot be explained by a strain dependence of r because it causes a decrease in strain sensitivity in high fields. However, an increase of just ~ 5% in d for a tensile strain of 1 % explains the increasing strain sensitivity shown by the 77 K, B //*c*-axis data in figure 4(d). Nevertheless without data at much higher fields we cannot determine whether this is due to changes in B_{c2} (which has been observed[53]) or s.

The r parameter (shown in Table 1) is unity and temperature independent for both Nb_3Sn and YBCO. These results imply that the resistivity of the grain boundaries and the grains in these materials have a similar temperature dependence and so are both metallic. For BiSCCO, r is small with a temperature dependence consistent with the grain boundaries being highly resistive and semiconducting. Although the ratio r/w is fixed when parameterising the BiSCCO J_c data, because the parameter w is strongly correlated with r and so can change without significant changes in the quality of fit, we have provided fits to the data with w set equal to that of YBCO. The presence of the parameter w in equation (5) explains why decreasing grain size was so effective in LTS materials and flux pinning theory has been so

useful, since (using the language of pinning) the edges of the junctions can be interpreted as pinning sites. Since w is a few microns in Nb_3Sn, about a factor of 5 – 10 larger than the grain size[54], it suggests that several grains act together as a single channel or equivalently not all triple points separate the channels (probably because they are not aligned sufficiently with the field direction). The HTS YBCO and BiSCCO have much smaller values of w than the grain sizes in these materials [55-57] which implies that faceting or grain boundary dislocations divide a grain boundary into many SNS junctions, or to use the language of flux pinning, there are strong pinning sites along the grain boundaries[41, 58, 59]. In parameterising the free-parameter d, we need only introduce the constant d_0 to describe the BiSCCO J_c data and even in this case d_0 is sufficiently small that it only significantly affects d at the very lowest temperatures where the fundamental superconducting properties are least well known. Simple arguments can provide an explanation for the s-values found: s is small in YBCO because B_{c2} is not dependent on strain and the low angle grain boundaries are thin; s is larger in Nb_3Sn because the mechanism that causes superconductivity is different in LTS from HTS so unlike YBCO, strain depresses the superconductivity near the grain boundaries[32] and s is largest in BiSCCO because the PIT route produces relatively large angle grain boundaries. Detailed compositional, structural and electronic information near the grain boundaries will be necessary to provide a more detailed explanation for the s values measured here.

5. CHANNELS AND ARTIFICIAL PINNING IN SUPERCONDUCTORS

This work shows that channels are an essential component of a proper description of J_c in polycrystalline superconductors. The mathematical framework described, helps to characterise local grain boundary properties from J_c measurements, unifies our understanding of J_c in LTS and HTS and informs new grain boundary engineering strategies for improving J_c in both LTS and HTS. For polycrystalline materials, equations (5) and (6) most obviously describe channels formed by grain boundaries. Long-standing literature developed to explain the field dependence of J_c in HTS materials proposes two different mechanisms to separately explain the power law dependence by pinning and the exponential dependence by thermally activated pinning (i.e. flux creep) of vortices in the bulk[60, 61]. However, these historical models are flux pinning models which cannot describe the strain dependence of J_c in YBCO reported here. This paper uses a single functional form that naturally leads to power law behaviour at low field and exponential behaviour in high fields without introducing two mechanisms. Although the model presented here described by equations (5) and (6) seems to be mathematically more daunting than the flux pinning equation given in equation (1), the number of free parameters is not significantly different. Comparing (1) with (5) and (6), the parameters n, p and q in (1) are effectively replaced by s and the parameters α and D by w. If the results $d_0 = 0$ and $r =$

1 found here for Nb_3Sn and YBCO are generally true for metallic superconductors with well-connected grains, there is actually a reduction in the number of parameters required to specify the functional form of J_c. This reduction will help magnet engineers assess the merits of the many different superconducting materials available for applications.

Significant improvements in YBCO[62] and BiSCCO[63] have been achieved by heavily loading these materials with artificial pinning (AP). In YBCO, ion irradiation[62] and nanodots[64] have been successful. More recently, self-assembling nano-columns have also been very effective in increasing J_c which are aligned along the c-axis of the material and have helped reduce the angular variation (i.e. anisotropy) in J_c as a function of the direction of the applied field[65, 66]. In this context, it is helpful to consider a range of different microstructures determining J_c, from those materials with isolated pinning sites, those with pinning sites joined by shallow channels and those with joined-up deep channels alone. Even in high J_c quasi-single crystal thin films with large low-angle (non-planar) grain boundaries, we can expect that when the density of dislocations is sufficiently high, some (small) parts of the film consist of channels made up of chains of dislocations. Until we know the mechanism that causes superconductivity, it is difficult to know the spatial extent of the disruption in superconductivity near a dislocation (for example from local changes in the electronic band-structure or composition) or what maximum dislocation separation retains overlap and provide channels for flux flow. Indeed this knowledge-deficit hinders us more generally from relating the structure and composition of superconducting materials (i.e. electron microscopy data) to their transport properties (i.e. J_c data). The power-law/exponential field dependence of J_c found for example in some high dislocation density single crystal thin films (with few grain boundaries) of YBCO [60, 67, 68] or some very high J_c BiSCCO[61] materials, provides evidence that flux flows along channels. We suggest that in order to parameterise $J_c(B,T,\varepsilon,\vartheta)$ comprehensively in such materials with pinning and channels, one may usefully introduce an anisotropy in (or angular dependence to) the width (w) of the channels that competes with the intrinsic anisotropy of the HTS material itself. Whether AP is practical for improving LTS polycrystalline materials is still an open question, but increasingly we can expect state-of-the-art HTS materials to have both channels and multiple types of AP operating[69]. In future there will be the real challenges of identifying what multiple processes are limiting J_c in such complex materials and how to parameterise J_c.

6. CONCLUDING COMMENTS

Flux pinning theory can provide important insights into how J_c arises and is particularly useful if the pinning sites are well separated and the number of fluxons is very small. However, it cannot describe the strain dependence of J_c in YBCO reported here. Historically, the isotope effect led to an understanding of the phonon-mediated fundamental mechanism in LTS superconductors and phonons provided an explanation for the strain dependence of B_{c2} in the LTS Nb_3Sn[48]. The evidence that strain does not affect the average superconducting properties

of YBCO may yet provide an important insight into the mechanism that gives rise to superconductivity in HTS[70, 71].

Acknowledgements

We are grateful to Professor Osamura (RIAS) and Drs. Sato and Fujikami (Sumitomo Electric Industries Ltd) for providing the multifilamentary DI-BiSCCO type HT tapes and acknowledge important discussions with them. This work was supported by EPSRC (Grant: EP/C535758/1) and a Royal Government of Thailand (DPST) PhD Scholarship.

Tables

	$r(T=0)$	w	s	T_c	d_0
Nb_3Sn	1.0	4.2 μm	1.9	16.2 K	0
YBCO	1.0	122 nm	1.2	87.6 K	0
BiSCCO	3.6×10^{-2}	122 nm	6.0	110.8 K	2.0 nm

Table 1: The parameters $r(T=0)$, w, s , T_c and d_0 for Nb_3Sn, YBCO and BiSCCO fitted to the J_c data using equations (5) and (6).

Figures

a

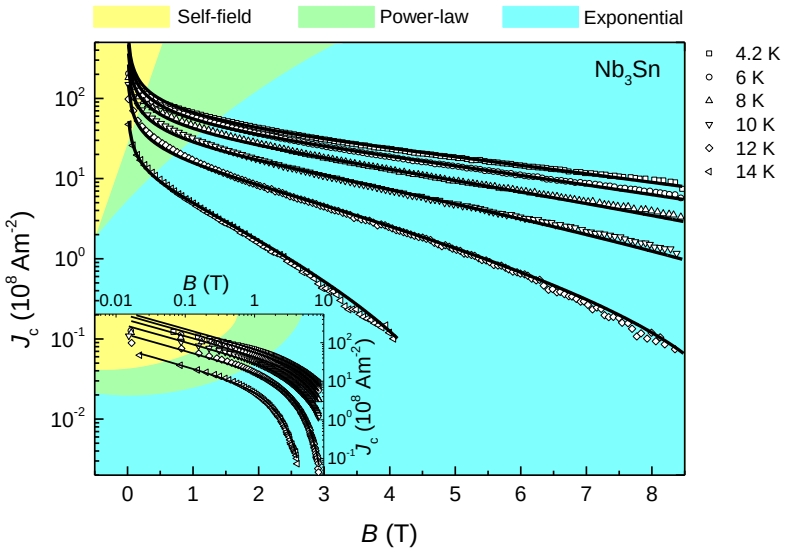
Self-field
Power-law
Exponential
Nb3Sn
4.2 K
6 K
8 K
10 K
12 K
14 K
Jc (10^8 Am^-2)
B (T)
B (T)
Jc (10^8 Am^-2)

b

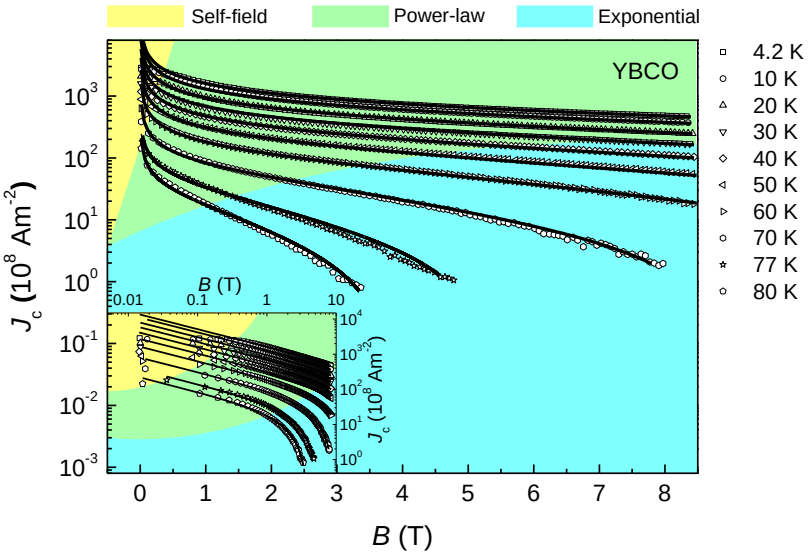
Self-field
Power-law
Exponential
YBCO
4.2 K
10 K
20 K
30 K
40 K
50 K
60 K
70 K
77 K
80 K
Jc (10^8 Am^-2)
B (T)
B (T)
Jc (10^8 Am^-2)

c

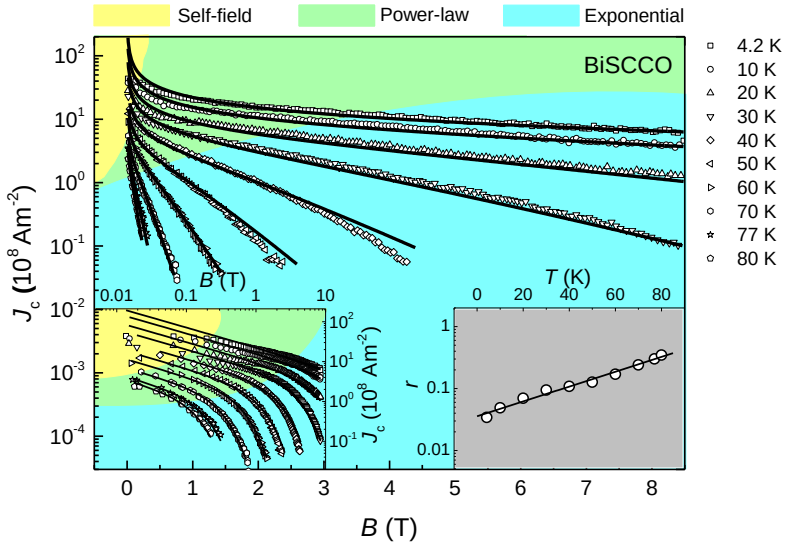

Figure 1: Three regimes of magnetic field dependence of the critical current density.

a, Log-linear plots of magnetisation critical current density versus magnetic field calculated using Bean's critical state model [19] for a Nb_3Sn wire, showing the self-field regime (yellow), power-law behaviour (green) and exponential behaviour (blue). The inset is a log-log plot of the same data, showing power-law behaviour in low fields. **b, c.** Similar plots for YBCO and BiSCCO for the field parallel to the c-axis of the tape. In **c**, an additional inset shows the temperature dependence of r consistent with semiconducting behaviour of the BiSCCO grain boundaries. Solid lines are fits to equations (5) and (6).

a

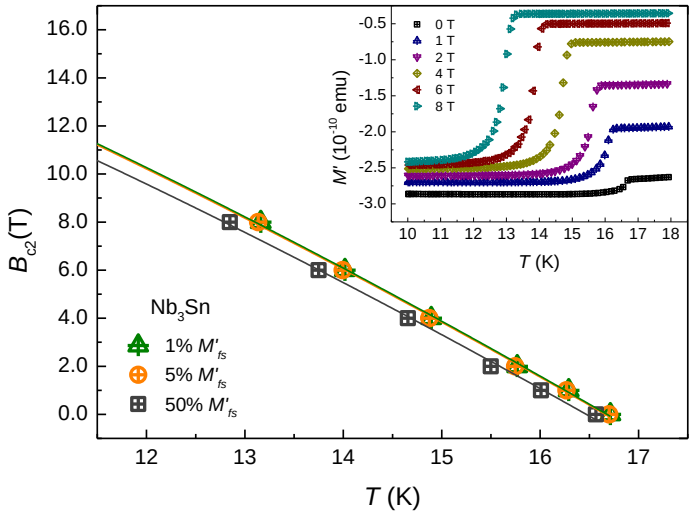
B_{c2} (T)
T (K)
Nb_3Sn
1% M'_{fs}
5% M'_{fs}
50% M'_{fs}
M' (10^{-10} emu)
0 T
1 T
2 T
4 T
6 T
8 T

b

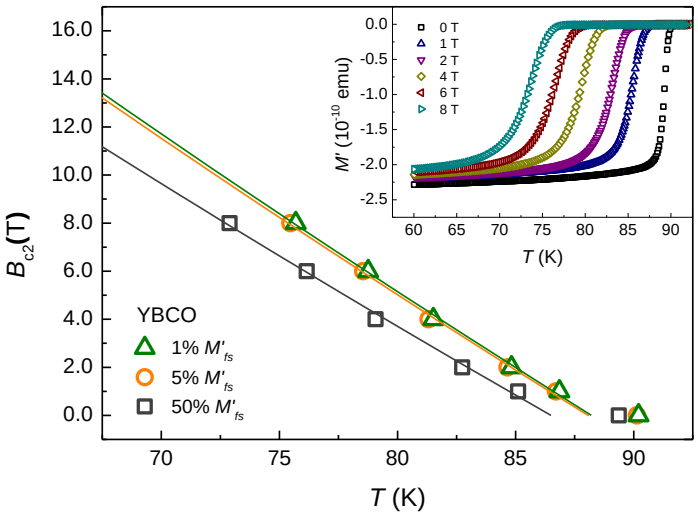
B_{c2}(T)
T (K)
YBCO
1% M'_{fs}
5% M'_{fs}
50% M'_{fs}
M' (10^{-10} emu)
0 T
1 T
2 T
4 T
6 T
8 T

c

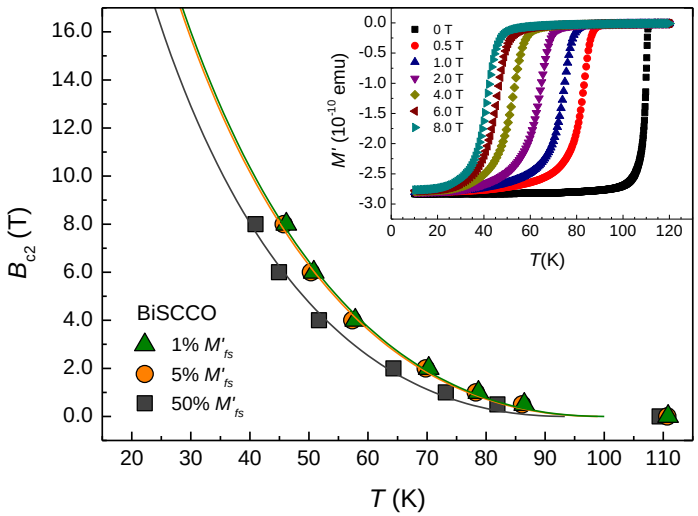
B_{c2} (T)
T (K)
BiSCCO
1% M'_{fs}
5% M'_{fs}
50% M'_{fs}
M' (10^{-10} emu)
0 T
0.5 T
1.0 T
2.0 T
4.0 T
6.0 T
8.0 T
T(K)

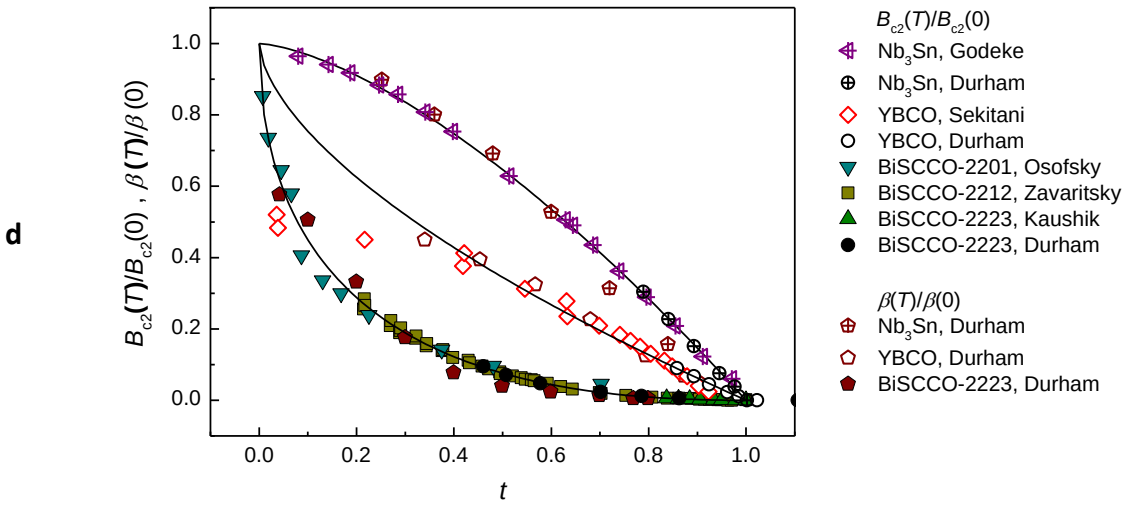

Figure 2: Temperature dependence of the upper critical magnetic field. a, Upper critical field of Nb_3Sn versus temperature obtained from ac magnetic susceptibility measurements that are shown in the inset. The upper critical magnetic field is shown at 1%, 5% and 50% of full screening (M'_{fs}). The solid lines are fits to the in-field data with $B_{c2}(T) = B_{c2}(0)(1\text{-}t^{1.5})$, giving the values of $B_{c2}(0)[T_c]$ of 26.3 T [16.7 K], 26.3 T [16.7 K] and 25.3 T [16.5K]. **b,** Equivalent YBCO data with the field applied along the c-axis of the tape. The solid lines are fits to the data with $B_{c2}(T) = B_{c2}(0)(1\text{-}t^{0.61})$, giving the values of $B_{c2}(0)[T_c]$ of 89.0 T [88.2 K], 88.2 T [88.1 K] and 79.6 T [86.5K]. **c,** Equivalent BiSCCO data where the solid line fits are $B_{c2}(T) = B_{c2}(0)(1\text{-}t^{0.5})^{2.1}$, with fitting parameters of 84.5 T [100.2 K], 83.7 T [99.7 K] and 74.4 T [93.7 K] respectively. **d,** Normalised B_{c2} and β as a function of reduced temperature for Nb_3Sn, YBCO and BiSCCO. Durham's B_{c2} data are taken from **a**, **b** and **c** at 1% M'_{fs}. Durham's β data are taken from the magnetisation critical current density in figure 1 fitted in the high field regime. $\beta(0)$ for Nb_3Sn, YBCO and BiSCCO are 6.8 T, 23.4 T and 13.5 T respectively. The lines describe the reduced temperature relations for $B_{c2}(T)$ given in **a**, **b** and **c** that were obtained from fits to the J_c data where $B_{c2}(0)[T_c]$ are 26.3 T [16.2 K], 68.5 T [87.6 K] and 84.5 T [110.8 K] respectively. The data from the literature are from Godeke[33], Sekitani[34], Osofsky[35], Zavaritsky[36] and Kaushik[37].

a

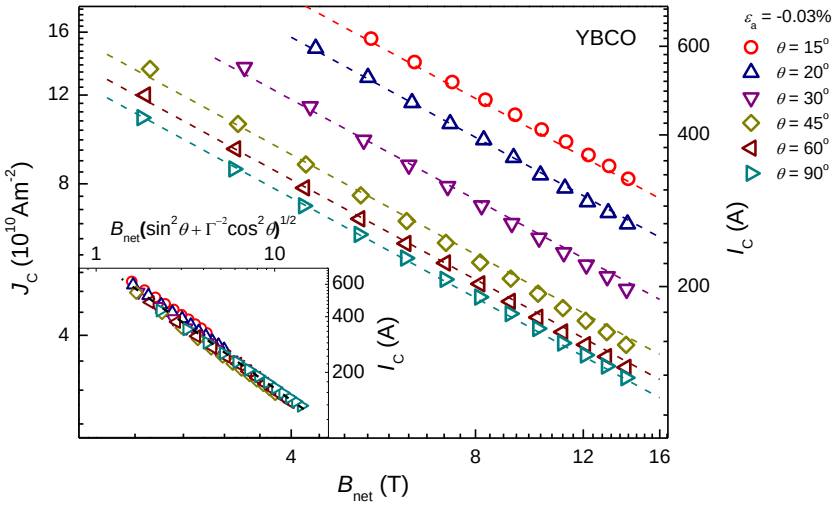
YBCO
ε_a = -0.03%
θ = 15°
θ = 20°
θ = 30°
θ = 45°
θ = 60°
θ = 90°
J_C (10^{10} Am^{-2})
I_C (A)
B_{net} (T)
$B_{net}(\sin^2\theta+\Gamma^{-2}\cos^2\theta)^{1/2}$

b

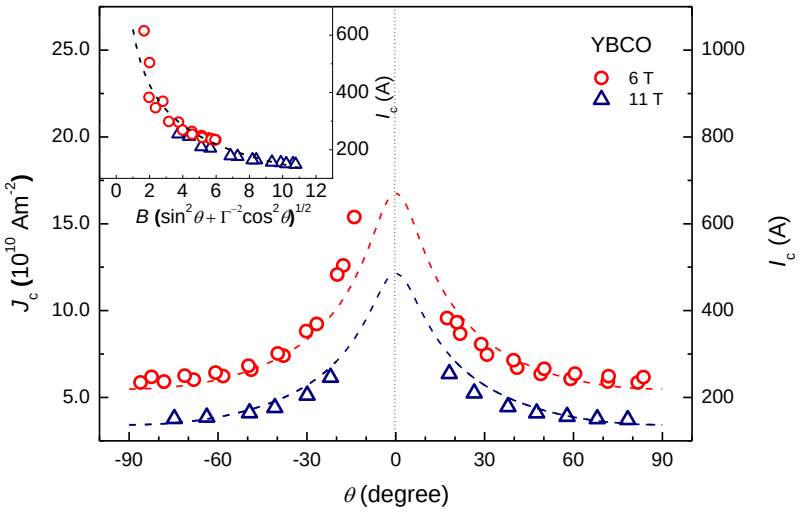
YBCO
6 T
11 T
J_c (10^{10} Am^{-2})
I_c (A)
θ (degree)
$B(\sin^2\theta+\Gamma^{-2}\cos^2\theta)^{1/2}$

c

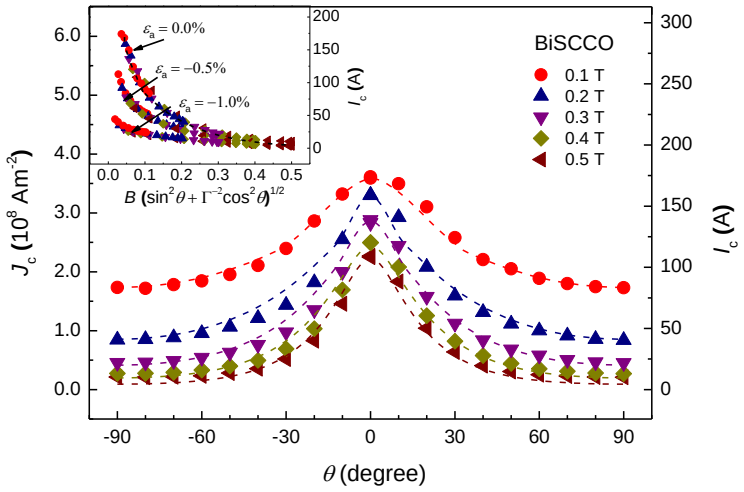
BiSCCO
0.1 T
0.2 T
0.3 T
0.4 T
0.5 T
ε_a = 0.0%
ε_a = −0.5%
ε_a = −1.0%
J_c (10^8 Am^{-2})
I_c (A)
θ (degree)
$B(\sin^2\theta+\Gamma^{-2}\cos^2\theta)^{1/2}$

Figure 3: Anisotropic properties of YBCO and BiSCCO. a¸ Transport critical current density of a YBCO tape at 4.2 K versus field at different angles between magnetic field and the tape surface. **Inset,** Data replotted as a universal curve versus $B \cdot (\sin^2\theta + \Gamma^{-2}\cos^2\theta)^{1/2}$ where Γ is 7.0. **b,** Transport critical current density of YBCO at 4.2 K versus angle between magnetic field and the tape surface at 6 T and 11 T. **Inset,** Data replotted as a universal curve where Γ is 7.0 **c,** Transport critical current density of BiSCCO tapes at 77 K versus angle between magnetic field and the tape surface for zero applied strain. **Inset,** Data replotted as a universal curve as well as data at two other strains where Γ is 7.8. Dotted lines are guides to the eye.

a

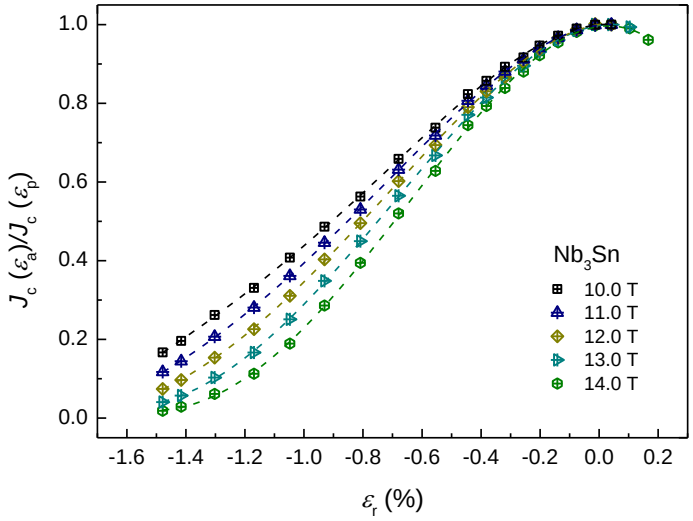
Nb3Sn
10.0 T
11.0 T
12.0 T
13.0 T
14.0 T
Jc (εa)/Jc (εp)
εr (%)

b

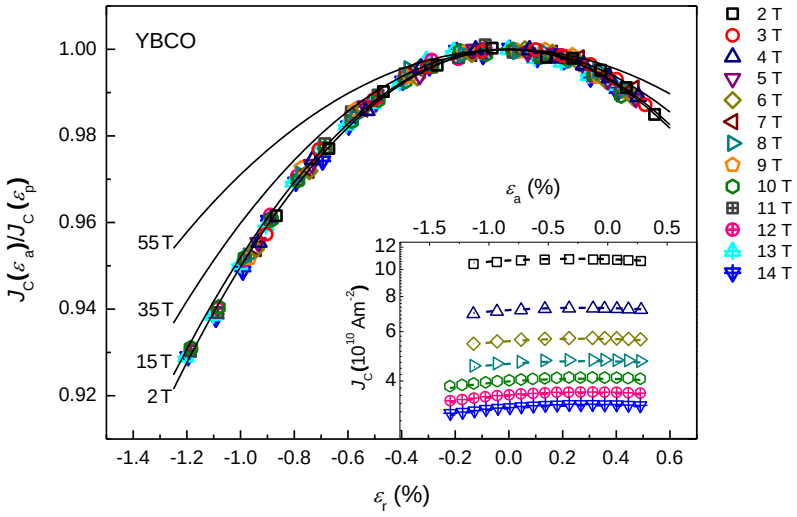
YBCO
55T
35T
15T
2T
2 T
3 T
4 T
5 T
6 T
7 T
8 T
9 T
10 T
11 T
12 T
13 T
14 T
εa (%)
JC(10^10 Am^-2)
JC(εa)/JC(εp)
εr (%)

c

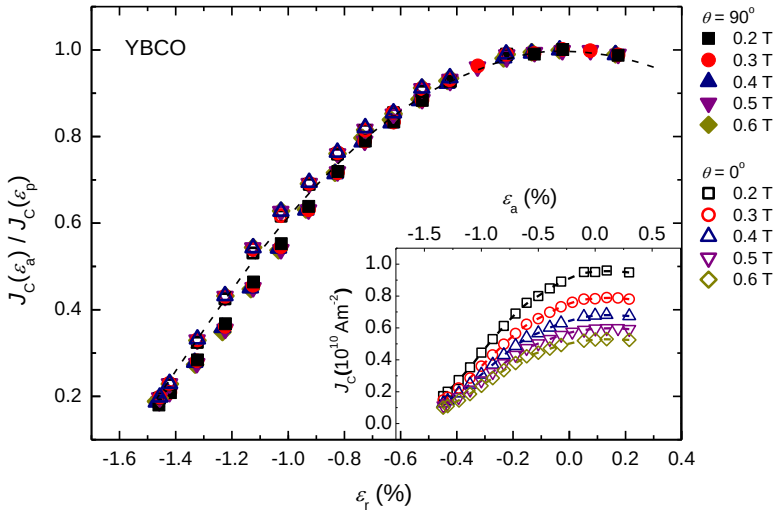
YBCO
θ = 90°
0.2 T
0.3 T
0.4 T
0.5 T
0.6 T
θ = 0°
0.2 T
0.3 T
0.4 T
0.5 T
0.6 T
εa (%)
JC(10^10 Am^-2)
JC(εa) / JC(εp)
εr (%)

d

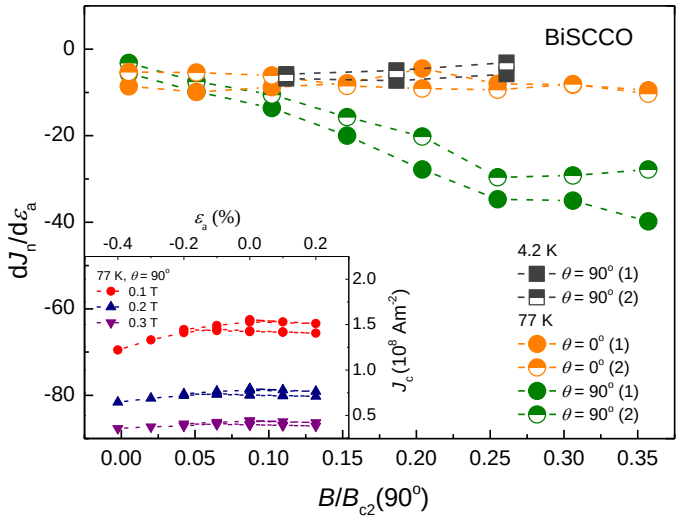

Figure 4: Effect of strain on the critical current density. a, Normalised critical current density, $J_n = J_c(\varepsilon_a)/J_c(\varepsilon_p)$ of a Nb_3Sn wire versus relative strain at 4.2 K for different applied magnetic fields. **b**, Current density of a YBCO tape versus applied strain (inset). Normalised critical current density of YBCO versus relative strain at 4.2 K at different magnetic fields applied parallel to the *c*-axis. $J_n(\varepsilon)$ shows power-law magnetic field behaviour and ε_p is a weak function of field. Also shown as solid lines are calculations of J_c at very high fields **c**, Critical current density of a YBCO tape versus applied strain at 77 K for different fields applied parallel to the surface of the tape (inset). J_n of YBCO versus relative strain at 77 K at different magnetic fields applied parallel and orthogonal to the c-axis. **d**, J_c versus strain for a BiSCCO tape (inset). $dJ_n/d\varepsilon_a$ as a function of reduced magnetic field for the $B//c$-axis orientation ($B/B_{c2}(90^o)$) for BiSCCO at 4.2 K and 77 K for two different orientations of magnetic field. Only reversible J_c data were used to obtain $dJ_n/d\varepsilon_a$. (1) and (2) represent the 1st and the 2nd reversible lines as seen in the inset. Dotted lines are guides to the eye.

1. SCHAUER, W. & SCHELB, W. IMPROVEMENT OF Nb_3Sn HIGH FIELD CRITICAL CURRENT BY A TWO-STAGE REACTION. *IEEE TRANS. MAGN.* **17**, 374-377 (1981).

2. DEW-HUGHES, D. FLUX PINNING MECHANISMS IN TYPE II SUPERCONDUCTORS. *PHILOS. MAG.* **30**, 293-305 (1974).

3. FLUKIGER, R. *ET AL*. OPTIMIZATION OF Nb_3Sn AND MgB_2 WIRES. *SUPERCONDUCTOR SCIENCE & TECHNOLOGY* **21**, 054015 (2008).

4. BONNEY, L.A., WILLIS, T.C. & LARBALESTIER, D.C. DEPENDENCE OF CRITICAL CURRENT DENSITY ON MICROSTRUCTURE IN THE $SnMo_6S_8$ CHEVREL-PHASE SUPERCONDUCTOR. *J. APPL. PHYS.* **77**, 6377-6387 (1995).

5. ROSSI, L. SUPERCONDUCTIVITY: ITS ROLE, ITS SUCCESS AND ITS SETBACKS IN THE LARGE HADRON COLLIDER OF CERN. *SUPERCOND. SCI. TECH.* **23**, 034001 (2010).

6. DIMOS, D., CHAUDHARI, P., MANNHART, J. & LEGOUES, F.K. ORIENTATION DEPENDENCE OF GRAIN-BOUNDARY CRITICAL CURRENTS IN $YBa_2Cu_3O_{7-\Delta}$ BICRYSTALS. *PHYS. REV. LETT.* **61**, 219-222 (1988).

7. HILGENKAMP, H. & MANNHART, J. GRAIN BOUNDARIES IN HIGH-T_C SUPERCONDUCTORS. *REV. MOD. PHYS.* **74**, 485-549 (2002).

8. HSIANG, T.Y. & FINNEMORE, D.K. SUPERCONDUCTING CRITICAL CURRENTS FOR THICK, CLEAN SUPERCONDUCTOR-NORMAL-METAL-SUPERCONDUCTOR JUNCTIONS. *PHYS. REV. B* **22**, 154-163 (1980).

9. LARBALESTIER, D.C. *ET AL*. WEAK LINKS AND THE POOR TRANSPORT CRITICAL CURRENTS OF THE 123 COMPOUNDS. *PHYSICA C* **153-155**, 1580-1585 (1988).

10. CARTY, G. & HAMPSHIRE, D.P. VISUALISING THE MECHANISM THAT DETERMINES THE CRITICAL CURRENT DENSITY IN POLYCRYSTALLINE SUPERCONDUCTORS USING TIME-DEPENDENT GINZBURG-LANDAU THEORY. *PHYS. REV. B* **77**, 172501 (2008).

11. CARTY, G.J. & HAMPSHIRE, D.P. THE CRITICAL CURRENT DENSITY OF AN SNS JUNCTION IN HIGH MAGNETIC FIELDS. *SUST* **26**, 065007 (2013).

12. TINKHAM, M. *INTRODUCTION TO SUPERCONDUCTIVITY*, EDN. 2ND. (MCGRAW-HILL BOOK CO., SINGAPORE; 1996).

13. POOLE, C.P., FARACH, H.A. & CRESWICK, R.J. *SUPERCONDUCTIVITY*. (ACADEMIC PRESS INC, SAN DIEGO, CALIFORNIA; 1995).

14. SCHMID, A. A TIME DEPENDENT GINZBURG-LANDAU EQUATION AND ITS APPLICATION TO THE PROBLEM OF RESISTIVITY IN THE MIXED STATE. *PHYSIK DER KONDENSIERTE MATERIE* **5**, 302-317 (1966).

15. NIKULOV, A.V. & REMISOV, Y.D. THE CRITICAL CURRENT OF THE JOSEPHSON JUNCTION WITH BOUNDARIES IN THE MIXED STATE: APPLICATION TO HTSC POLYCRYSTALLINE MATERIALS. *SUPERCOND. SCI. TECH.* **3**, 312-317 (1991).

16. BARONE, A. & PATERNO, G. *PHYSICS AND APPLICATIONS OF THE JOSEPHSON EFFECT*. (WILEY, NEW YORK; 1982).

17. CASTRO, H. *ET AL*. TUNNELING SPECTROSCOPY: A PROBE FOR HIGH-TC SUPERCONDUCTIVITY. *MICROELECTRONICS JOURNAL* **39**, 1296-1299 (2008).

18. DE GENNES, P.G. *SUPERCONDUCTIVITY OF METALS AND ALLOYS*. (ADDISON WESLEY PUBLISHING COMPANY, REDWOOD CITY, CALIFORNIA; 1989).

19. BEAN, C.P. MAGNETIZATION OF HIGH-FIELD SUPERCONDUCTORS. *REV. MOD. PHYS.* **36**, 31-39 (1964).

20. WALTERS, C.R., DAVIDSON, I.M. & TUCK, G.E. LONG SAMPLE HIGH SENSITIVITY CRITICAL CURRENT MEASUREMENTS UNDER STRAIN. *CRYOGENICS* **26**, 406-412 (1986).

21. CHEGGOUR, N. & HAMPSHIRE, D.P. A PROBE FOR INVESTIGATING THE EFFECTS OF TEMPERATURE, STRAIN, AND MAGNETIC FIELD ON TRANSPORT CRITICAL CURRENTS IN SUPERCONDUCTING WIRES AND TAPES. *REV. SCI. INSTRUM.* **71**, 4521-4530 (2000).

22. SUNWONG, P., HIGGINS, J.S. & HAMPSHIRE, D.P. ANGULAR, TEMPERATURE AND STRAIN DEPENDENCIES OF THE CRITICAL CURRENT OF DI-BSCCO TAPES IN HIGH MAGNETIC FIELDS. *IEEE TRANS. APPL. SUPERCOND.* **21**, 2840-2844 (2011).

23. HIGGINS, J.S. & HAMPSHIRE, D.P. CRITICAL CURRENT DENSITY OF $YBa_2Cu_3O_{7-\Delta}$ COATED CONDUCTORS UNDER HIGH COMPRESSION IN HIGH FIELDS. *IEEE TRANS. APPL. SUPERCOND.* **21**, 3234-3237 (2011).

24. HAMPSHIRE, D.P. A BARRIER TO INCREASING THE CRITICAL CURRENT DENSITY OF BULK UNTEXTURED POLYCRYSTALLINE SUPERCONDUCTORS IN HIGH MAGNETIC FIELDS. *PHYSICA C* **296**, 153-166 (1998).

25. BULAEVSKII, L.N., DAEMEN, L.L., MALEY, M.P. & COULTER, J.Y. LIMITS TO THE CRITICAL CURRENT IN HIGH-TC SUPERCONDUCTING TAPES. *PHYS. REV. B* **48**, 798 (1993).

26. LE LAY, L., FRIEND, C.M., MARUYAMA, T., OSAMURA, K. & HAMPSHIRE, D.P. EVIDENCE THAT PAIR BREAKING AT THE GRAIN BOUNDARIES OF BI2SR2CA2CU3OX TAPES DETERMINES THE CRITICAL CURRENT DENSITY ABOVE 10 K IN HIGH FIELDS. *J. PHYS.:CONDENS MATTER* **6**, 10053-10066 (1994).

27. MAWATARI, Y., YAMASAKI, H., KOSAKA, S. & UMEDA, M. CRITICAL CURRENT PROPERTIES AND VORTEX-GLASS-LIQUID-TRANSITION IN AG-SHEATHED BI-2223 TAPES. *CRYOGENICS* **35**, 161-167 (1995).

28. DHALLE, M. *ET AL*. EXPERIMENTAL ASSESMENT OF THE CURRENT-LIMITING MECHANISMS IN BSCC0/AG HIGH TEMPERATURE SUPERCONDUCTING TAPES. *SUPERCONDUCTOR SCIENCE & TECHNOLOGY* **10**, 21-31 (1997).

29. HAMPSHIRE, D.P. & CHAN, S.-W. THE CRITICAL CURRENT DENSITY IN HIGH FIELDS IN EPITAXIAL THIN FILMS OF $YBa_2Cu_3O_7$: FLUX PINNING AND PAIR-BREAKING. *J. APPL. PHYS.* **72**, 4220-4226 (1992).

30. AYMAR, R. ITER R&D: EXECUTIVE SUMMARY: DESIGN OVERVIEW. *FUSION ENG. DES.* **55**, 107-118 (2001).

31. WERTHAMER, N.R., HELFAND, E. & HOHENBERG, P.C. TEMPERATURE AND PURITY DEPENDENCE OF THE SUPERCONDUCTING CRITICAL FIELD, H_{C2}. III. ELECTRON SPIN AND SPIN-ORBIT EFFECTS. *PHYS. REV.* **147**, 295-302 (1966).

32. CHEGGOUR, N. & HAMPSHIRE, D.P. THE UNIFIED STRAIN AND TEMPERATURE SCALING LAW FOR THE PINNING FORCE DENSITY OF BRONZE-ROUTE Nb_3Sn WIRES IN HIGH MAGNETIC FIELDS. *CRYOGENICS* **42**, 299 - 309 (2002).

33. GODEKE, A., JEWELL, M.C., GOLUBOV, A.A., TEN HAKEN, B. & LARBALESTIER, D.C. INCONSISTENCIES BETWEEN EXTRAPOLATED AND ACTUAL CRITICAL FIELDS IN Nb_3Sn WIRES AS DEMONSTRATED BY DIRECT MEASUREMENTS OF H_{C2}, H^* AND T_C. *SUPERCOND. SCI. TECH.* **16**, 1019-1025 (2003).

34. SEKITANI, T. UPPER CRITICAL FIELD FOR OPTIMALLY-DOPED $YBa_2Cu_3O_{7-\Delta}$. *PHYSICA B* **346-347**, 319-324 (2004).

35. OSOFSKY, M.S. *ET AL*. ANOMALOUS TEMPERATURE DEPENDENCE OF THE UPPER CRITICAL MAGNETIC FIELD IN BI-SR-CU-0. *PHYS. REV. LETT.* **71**, 2315 (1993).

36. ZAVARITSKY, V.N., SPRINGFORD, M. & ALEXANDROV, A.S. C-AXIS NEGATIVE MAGNETORESISTANCE AND UPPER CRITICAL FIELD OF $Bi_2Sr_2CaCu_2O_Y$. *EUROPHYS. LETT.* **51**, 334 (2000).

37. KAUSHIK, S.D. & PATNAIK, S. INTERGRAIN CONNECTIVITY AND RESISTIVE BROADENING IN VORTEX STATE: A COMPARISON BETWEEN MgB_2, $NbSe_2$ AND $Bi_2Sr_2Ca_2Cu_3O_{10}$ SUPERCONDUCTORS. *IEEE TRANS. APPL. SUPERCOND.* **17**, 3016-3019 (2007).

38. CLEM, J. ANISOTROPY AND TWO-DIMENSIONAL BEHAVIOUR IN THE HIGH-TEMPERATURE SUPERCONDUCTORS. *SUPERCONDUCTOR SCIENCE & TECHNOLOGY* **11**, 909-914 (1998).

39. LAWRENCE, W.E. & DONIACH, S. IN PROCEEDINGS OF THE TWELTH INTERNATIONAL CONFERENCE ON LOW TEMPERATURE PHYSICS. (ED. E. KANDA) 361 (ACADEMIC PRESS OF JAPAN, KYOTO; 1971).

40. HOGG, M.J., KAHLMANN, F., BARBER, Z.H. & EVETTS, J.E. ANGULAR HYSTERESIS IN THE CRITICAL CURRENT OF $YBa_2Cu_3O_7$ LOW-ANGLE GRAIN BOUNDARIES. *SUPERCONDUCTOR SCIENCE & TECHNOLOGY* **14**, 647-650 (2001).

41. LARBALESTIER, D.C., GUREVICH, A., FELDMANN, D.M. & POLYANSKII, A. HIGH -T_C SUPERCONDUCING MATERIALS FOR ELECTRIC POWER APPLICATIONS. *NATURE* **414**, 368-377 (2001).

42. HAO, Z. ANGULAR DEPENDENCES OF THE THERMODYNAMIC AND ELECTROMAGNETIC PROPERTIES OF THE HIGH-T_C SUPERCONDUCTORS IN THE MIXED STATE. *PHYS. REV. B* **46**, 5853-5856 (1992).

43. SNEARY, A.B. THE FABRICATION OF A HIGH TEMPERATURE SUPERCONDUCTING MAGNET AND CRITICAL CURRENT CHARACTERISATION OF THE COMPONENT $Bi_2Sr_2Ca_2Cu_3O_X$ TAPES AND FILAMENTS IN HIGH MAGNETIC FIELDS. *THESIS: DEPARTMENT OF PHYSICS, DURHAM UNIVERSITY*, 1-156 (2000).

44. TAGAYA, K., SENDA, K., YOSIDA, T., FUKUOKA, N. & SASAKURA, H. LOWER CRITICAL FIELDS IN BI-2212 AND BI-2223 SUPERCONDUCTORS. *JAP. J. APPL. PHYS.* **31**, L 1170-L 1171 (1992).

45. MATSUBARA, I., TANIGAWA, H., OGURA, T., YAMASHITA, H. & KINOSHITA, M. UPPER CRITICAL FIELD AND ANISOTRPY OF THE HIGH-TC BSCCO PHASE. *PHYS. REV. B* **45**, 7414-7417 (1992).

46. CYROT, M. & PAVUNA, D. *INTRODUCTION TO SUPERCONDUCTIVITY AND HIGH-TC MATERIALS*. (WORLD SCIENTIFIC, SINGAPORE; 1992).

47. MARTÍNEZ, J.C. *ET AL*. MAGNETIC ANISOTROPY OF A $Bi_2Sr_2CaCu_2O_x$ SINGLE CRYSTAL. *PHYS. REV. LETT.* **69**, 2276-2279 (1992).

48. TAYLOR, D.M.J. & HAMPSHIRE, D.P. THE SCALING LAW FOR THE STRAIN DEPENDENCE OF THE CRITICAL CURRENT DENSITY IN Nb_3Sn SUPERCONDUCTING WIRES. *SUPERCOND. SCI. TECH.* **18**, S241-S252 (2005).

49. SUGANO, M., SHIKIMACHI, K., HIRANO, N. & NAGAYA, S. THE REVERSIBLE STRAIN EFFECT ON CRITICAL CURRENT OVER A WIDE RANGE OF TEMPERATURES AND MAGNETIC FIELDS FOR YBCO COATED CONDUCTORS. *SUPERCONDUCTOR SCIENCE & TECHNOLOGY* **23**, 085013 (2010).

50. VAN DER LAAN, D.C. THE EFFECT OF STRAIN ON GRAIN BOUNDARIES IN $YBa_2Cu_3O_{7-\Delta}$ COATED CONDUCTORS. *SUPERCONDUCTOR SCIENCE & TECHNOLOGY* **23**, 014004 (2010).

51. VAN DER LAAN, D.C., HAUGAN, T.J. & BARNES, P.N. EFFECT OF A COMPRESSIVE UNIAXIAL STRAIN ON THE CRITICAL CURRENT DENSITY OF GRAIN BOUNDARIES IN SUPERCONDUCTING $YBa_2Cu_3O_7$ FILMS. *PHYS REV LETT* **103**, 027005 (2009).

52. WELP, U. *ET AL*. EFFECT OF UNIAXIAL STRESS ON THE SUPERCONDUCTING TRANSITION IN $YBa_2Cu_3O_7$. *PHYS REV LETT* **69**, 2130 (1992).

53. CHEN, X.F., TESSEMA, G.X. & SKOVE, M.J. EFFECT OF ELASTIC STRESS ON THE RESISTIVITY AND T_C OF $(Bi, Pb)_2Sr_2Ca_{N-1}Cu_NO_X$. *PHYSICA C* **181**, 340-344 (1991).

54. PUGH, N., EVETTS, J. & WALLACH, E. A TRANSMISSION ELECTRON-MICROSCOPY STUDY OF BRONZE-PROCESSED Nb_3Sn AND $(Nb,Ta)_3Sn$ MULTIFILAMENTARY SUPERCONDUCTING WIRE. *J MATER SCI* **20**, 4521-4526 (1985).

55. FELDMANN, D.M., HOLESINGER, T.G., FEENSTRA, R. & LARBALESTIER, D. A REVIEW OF THE INFLUENCE OF GRAIN BOUNDARY GEOMETRY ON THE ELECTROMAGNETIC PROPETRIES OF POLYCRYSTALLINE $YBa_2Cu_3O_{7-X}$ FILMS. *J. AM. CERAM. SOC.* **91**, 1869 (2008).

56. AYAI, N. *ET AL*. PROGRESS IN PERFORMANCE OF DI-BSCCO FAMILY. *PHYSICA C* **468**, 1747 (2008).

57. HENSEL, B., GRASSO, G. & FLUKIGER, R. LIMITS TO THE CRITICAL CURRENT IN SUPERCONDUCTING $(Bi,Pb)_2Sr_2Ca_2Cu_3O_{10}$ SILVER-SHEATHED TAPES: THE RAILWAY-SWITCH MODEL. *PHYS. REV. B* **51**, 15456 (1995).

58. GUREVICH, A. & PASHITSKII, E.A. CURRENT TRANSPORT THROUGH LOW-ANGLE GRAIN BOUNDARIES IN HIGH-TEMPERATURE SUPERCONDUCTORS. *PHYS. REV. B* **57**, 13878-13893 (1998).

59. GOYAL, A. *ET AL*. TEXTURE FORMATION AND GRAIN BOUNDARY NETWORKS IN ROLLING ASSISTED BIAXIALLY TEXTURED SUBSTRATES AND IN EPITAXIAL YBCO FILMS ON SUCH SUBSTRATES. *MICRON* **30**, 463-478 (1999).

60. KLAASSEN, F.C. VORTEX PINNING BY NATURAL LINEAR DEFECTS IN THIN FILMS OF $YBa_2Cu_3O_{7-\Delta}$. *PHYS. REV. B* **64**, 184523 (2001).

61. YAMASAKI, H. *ET AL.* SCALING OF FLUX PINNING FORCE IN EPITAXIAL $Bi_2Sr_2Ca_2Cu_3O_X$ THIN FILMS. *PHYS. REV. LETT.* **70**, 3331-3334 (1993).

62. MATSUI, H. *ET AL.* 4-FOLD ENHANCEMENT IN THE CRITICAL CURRENT DENSITY OF $YBa_2Cu_3O_7$ FILMS BY PRACTICAL ION IRRADIATION. *APPL PHYS LETT* **101**, 232601 (2012).

63. YANG, P. & LIEBER, C.M. NANOSTRUCTURED HIGH-TEMPERATURE SUPERCONDUCTORS: CREATION OF STRONG-PINNING COLUMNAR DEFECTS IN NANOROD/SUPERCONDUCTOR COMPOSITES. *J MATER RES* **12**, 2981-2996 (1997).

64. GUTIERREZ, J. *ET AL.* STRONG ISOTROPIC FLUX PINNING IN SOLUTION-DERIVED $YBa_2Cu_3O_{7-X}$ NANOCOMPOSITE SUPERCONDUCTOR FILMS. *NATURE MATERIALS* **6**, 367-373 (2007).

65. SELVAMANICKAM, V. *ET AL.* ENHANCED CRITICAL CURRENTS IN $(Gd,Y)Ba_2Cu_3O_X$ SUPERCONDUCTING TAPES WITH HIGH LEVELS OF ZR ADDITION. *SUPERCONDUCTIVITY SCIENCE AND TECHNOLOGY* **26**, 035006 (2013).

66. SELVAMANICKAM, V. *ET AL.* THE LOW-TEMPERATURE, HIGH-MAGNETIC-FIELD CRITICAL CURRENT CHARATCERISTICS OF ZR-ADDED $(Gd,Y)Ba_2Cu_3O_X$ SUPERCONDUCTING TAPES. *SUPERCONDUCTOR SCIENCE & TECHNOLOGY* **25**, 125013 (2012).

67. VAN DER BEEK, C.J. *ET AL.* STRONG PINNING IN HIGH-TEMPERATURE SUPERCONDUCTING FILMS. *PHYS. REV. B* **66**, 024523 (2002).

68. DAM, B. *ET AL.* ORIGIN OF HIGH CRITICAL CURRENTS IN $YBa_2Cu_3O_{7-D}$ SUPERCONDUCTING THIN FILMS. *NATURE* **399**, 439-442 (1999).

69. AYTUG, T. *ET AL.* NOVEL TRI-MODAL DEFECT STRUCTURE IN NB-DOPED MOCVD $YBa_2Cu_3O_7$: A PARADIGM FOR PINNING LANDSCAPE CONTROL. *SUPERCONDUCTIVITY SCIENCE AND TECHNOLOGY* **25**, 095013 (2012).

70. SHIMOJIMA, T. *ET AL.* ORBITAL-INDEPENDENT SUPERCONDUCTING GAPS IN IRON PNICTIDES. *SCIENCE* **332**, 564-567 (2011).

71. PARK, T. *ET AL.* ISOTROPIC QUANTUM SCATTERING AND UNCONVENTIONAL SUPERCONDUCTIVITY. *NATURE* **456**, 366-368 (2008).